Complex Impedance Transformers

©ISTOCKPHOTO.COM/GOVINDANMARUDHAI

Hee-Ran Ahn and Manos M. Tentzeris

With the development of wireless communication systems, the use of complex impedance transformers to convert one complex impedance into another is important for achieving the maximum power transfer. These transformers are exploited for impedance-transforming power dividers (PDs) and combiners [1]–[3], wireless power transfer [4] and energy harvesting, antenna feed lines, and power amplifiers. The simplest design is generally the most preferable for any engineering solution; thus, in most cases, the best approach is to use quarter-wave

Hee-Ran Ahn (hranahn@gmail.com) and Manos M. Tentzeris (etentze@ece.gatech.edu) are with the School of Electrical and Computer Engineering, Georgia Institute of Technology, Atlanta.

Digital Object Identifier 10.1109/MMM.2020.2998421
Date of current version: 3 August 2020

impedance transformers to convert one real impedance into another real impedance. However, since the input and output impedances of PDs [1]–[3]; transmitter- and receiver-coils for wireless power transfer systems [4]; and power transistors, antennas, and diodes for rectifiers are not always real values, complex impedance transformers are also needed to convert one complex impedance into another.

For this situation, diverse complex impedance transformers have been suggested, and they can be classified into six cases:

- The first consists of only one transmission-line section (TL) [5]–[9].
- The second includes one TL and stubs [10]–[12].
- The third incorporates two TLs and stubs [13]–[16].
- The fourth is composed of three TLs and stubs [17], [18].
- The fifth is made up of several TLs [19].
- The final one involves coupled TLs [20]–[24].

However, these conventional methods [5]–[27] can't treat all possible complex termination impedances, due to lack of an available systematic design method. Another issue is that these conventional designs tend to be unnecessarily complicated. Among the conventional methods, impedance transformers [5]–[10] with a single TL on each transformer are recommended due to their useful, simple, diverse applications and the possible implementation of all other conventional designs.

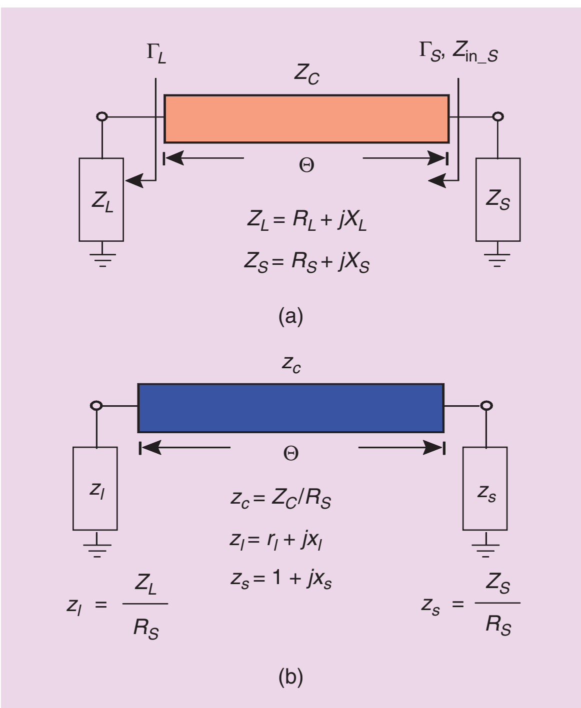

Figure 1. *Complex impedance transformers with only one TL. (a) The termination impedances without normalization. (b) The termination and characteristic impedances normalized to R_S.*

This article suggests impedance transformers with one TL for both complex termination impedances [28]; allowed and forbidden regions are defined in the impedance domain, and three mapping functions for the reflection coefficient domain (on a Smith chart) are derived. The *allowed region* is defined as an area where one TL can transform a complex impedance into another one, while the *forbidden region* is an area where the transformation with only one TL is impossible. Since Smith charts with both regions give at a glance all the information about the bandwidths [29]–[31], characteristic impedances, and electrical lengths [30], [31] of complex impedance transformers with one TL, they facilitate effective designs without any additional complicated calculation or derivation processes. To make all the complex termination impedances possible, even in the forbidden regions, a design method is illustrated using constant voltage-standing-wave-ratio (VSWR)-type transmission-line impedance transformers (CVTs) and constant-conductance-type transmission-line impedance transformers (CCTs) [31].

Next, to further verify the design methods and their usefulness, applications to various PDs are introduced. The impedance transformers of the PDs in [31] are designed using a graphical method on a Smith chart, and therefore applications do not seem easy to achieve. For better and easier use of the PDs in [31], complex impedance transformers with only one TL are employed. However, if the size of the circuit is small, the characteristic impedances of the impedance transformers are too high to be feasible in a microstrip format [29]–[31]. To alleviate this problem, small-phase-delay impedance transformers [32], [33] are introduced; however, the design method [32] is very complicated because full-port scattering parameters need to be applied.

This article discusses an easy design method using complex impedance transformers with only one TL. Furthermore, ultracompact and wideband impedance transformers [34] are treated, and a design method is introduced that uses complex impedance transformers with only one TL. In terms of size versus bandwidth, the fabricated PD [34] based on the low-cost microstrip technology discussed in the final section of the article may be regarded as the smallest ever recorded.

Complex Impedance Transformer With Only One TL

Impedance Domain Analyses

An impedance transformer terminated in complex termination impedances $Z_L = R_L + jX_L$ and $Z_S = R_S + jX_S$ is depicted in Figure 1(a), where R_L and R_S are positive real values and X_L and X_S are real values, including zero. It consists of only a single TL with the characteristic impedance of Z_C and the electrical length of Θ. If the two termination impedances are normalized to the real impedance R_S of Z_S, the normalized termination impedances are $z_l = Z_L/R_S$ and $z_s = Z_S/R_S$, and the characteristic impedance of the TL is also $z_c = Z_C/R_S$, as described in Figure 1(b). The reflection coefficients Γ_L and Γ_S and the input impedance of Z_{in_S} are indicated in Figure 1(a). Since the termination impedances Z_L and Z_S in Figure 1(a) can be located on a constant reflection-coefficient circle drawn on a Smith chart [5, Figs. 3(b) and 4(b)], the characteristic impedance of Z_C [5, eq. (2)] can be derived from the relation of $|\Gamma_L| = |\Gamma_S|$ as

$$Z_C = CH(Z_L, Z_S) = \sqrt{\frac{R_L|Z_S|^2 - R_S|Z_L|^2}{R_S - R_L}}, \qquad (1)$$

where Z_C should represent positive real values and $CH(Z_L, Z_S)$ is a function of Z_L and Z_S in Figure 1(a). The input impedance of Z_{in_S} in Figure 1(a) should be the same as Z_S^*, complex conjugate of Z_S, for the maximum power transfer, from which design formulas for the electrical length Θ [5], [7] can be derived as

$$\tan\Theta = EL(Z_L, Z_S) = Z_C\frac{R_L - R_S}{R_L X_S - R_S X_L}, \qquad (2)$$

where $EL(Z_L, Z_S)$ is a function that can provide the electrical length Θ when the two complex impedances of Z_L and Z_S in Figure 1(a) are given.

To treat all possible complex termination impedances, normalized termination impedances need to be discussed. Substituting $z_l = r_l + jx_l$ and $z_s = 1 + jx_s$ into (1) and (2) gives

$$z_c = \sqrt{\frac{r_l|z_s|^2 - |z_l|^2}{1 - r_l}}, \qquad (3a)$$

$$\tan\Theta = z_c\frac{r_l - 1}{r_l x_s - x_l}. \qquad (3b)$$

For the solution to z_c in (3a), z_c^2 should consist of positive real values, which leads to

$$0 < r_l < 1; \left(r_l - \frac{|z_s|^2}{2}\right)^2 + x_l^2 < \frac{|z_s|^4}{4}, \qquad (4a)$$

$$r_l > 1; \left(r_l - \frac{|z_s|^2}{2}\right)^2 + x_l^2 > \frac{|z_s|^4}{4}, \qquad (4b)$$

$$r_l = 1; \text{ no solution}, \qquad (4c)$$

where (4a) or (4b) is a circle equation with the center $(|z_s|^2/2, 0)$ and a radius of $|z_s|^2/2$. The regions satisfying the equations in (4) are demonstrated in Figure 2. Depending on the values of $|z_s|^2$, two cases of $|z_s|^2 > 1$ and $|z_s|^2 = 1$ are available, and no solution to z_c in (4c) exists when $r_l = 1$. The two cases with $|z_s|^2 > 1$ and $|z_s|^2 = 1$ are plotted in Figure 2(a) and (b), respectively, where the hatched areas show the allowed regions that permit the positive real characteristic impedances of z_c in (5a). That is, if a load of z_l is located in the allowed regions in Figure 2, only one TL can match z_l to z_s.

Reflection Coefficient Analyses

To define the allowed and forbidden regions on the Smith chart, three important functions can be defined as

$$f_1(r_l, x_l): \left(r_l - \frac{|z_s|^2}{2}\right)^2 + x_l^2 - \frac{|z_s|^4}{4} = 0, \qquad (5a)$$

$$f_2(r_l, x_l): r_l - 1 = 0, \qquad (5b)$$

$$f_3(r_l, x_l): r_l - \frac{x_l}{x_s} = 0. \qquad (5c)$$

The two functions in (5a) and (5b) are from (4), while the function in (5c) occurs when Θ is 90° in (3b). Using mapping functions to convert the impedance domain values of r_l and x_l into the reflection coefficient domain values of Γ_{rl} and Γ_{il} in [5, eq. (8)], three mapping functions for $f_1(r_l, x_l)$, $f_2(r_l, x_l)$, and $f_3(r_l, x_l)$ are derived as

$$G_{f1}: \left(\Gamma_{rl} + \frac{1}{1+|z_s|^2}\right)^2 + \Gamma_{il}^2 - \left(\frac{|z_s|^2}{1+|z_s|^2}\right)^2 = 0, \qquad (6a)$$

$$G_{f2}: \left(\Gamma_{rl} - \frac{1}{2}\right)^2 + \Gamma_{il}^2 - \left(\frac{1}{2}\right)^2 = 0, \qquad (6b)$$

$$G_{f3}: \Gamma_{rl}^2 + \left(\Gamma_{il} + \frac{1}{x_s}\right)^2 - \left(1 + \frac{1}{x_s^2}\right) = 0. \qquad (6c)$$

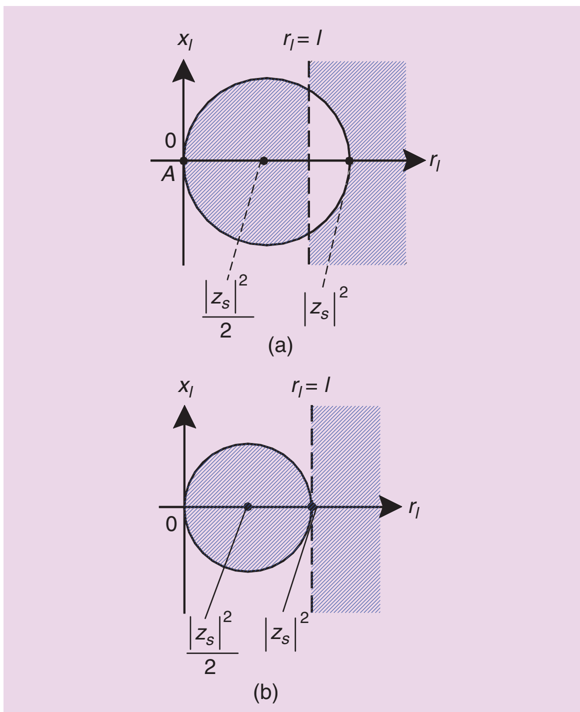

Figure 2. *The hatched allowed regions. (a) $|z_s|^2 > 1$. (b) $|z_s|^2 = 1$.*

The allowed regions on the Smith chart are $G_{f_1} < 0$ and $G_{f_2} > 0$ and $G_{f_1} > 0$ and $G_{f_2} < 0$.

CVTs and CCTs

Based on complex impedance transformers with only one TL, compact and wideband impedance transformers like CVTs and CCTs can be implemented. CVTs and CCTs are treated in [31] but may not be easy to understand because a graphical method on a Smith chart is applied for the solutions. Thus, a new interpretation may be helpful for readers.

CVTs and CCTs With Both Real Termination Impedances

A 90° impedance transformer to convert a real impedance of $z_l = r_l$ into another real one of $z_s = r_s = 1$ is depicted in Figure 3(a). If the operating frequency is low (fewer than 5 GHz), 90° impedance transformers are not small enough. To optimize wideband performance while reducing size, two types of small impedance transformers, CVT and CCT in Figure 3(b) and (c) with $r_l > 1$, respectively, can be implemented.

A half-immittance Smith chart is depicted in Figure 3(d), where impedance and admittance Smith charts are expressed with dark-green and red circles, respectively, and the values associated with the real axis are for the impedance Smith chart. Four half circles passing through $r = 2$ or $g = 0.5$ are drawn with different colors. The characteristic impedances of the blue, green, red, and dark-red half circles in Figure 3(d) are $z_c = 0.5\ \Omega$, $1\ \Omega$, $1.17\ \Omega$, and $1.41\ \Omega$, respectively, and the dark-red circle with $z_c = 1.41\ \Omega$ indicates the 90° impedance transformer to convert $r_l = 2$ into $r_s = 1$. All admittance values on the blue half circle with $z_c = 0.5$ are $0.5 + jx$, where x represents arbitrary positive values; therefore, the half circle is called *a constant-conductance circle*, while the others are defined as *constant-VSWR circles*.

To reduce the size of the 90° impedance transformer, the termination impedance $r_l = 2$ is moved along one of the constant-VSWR circles or a constant-conductance circle, leading to blue, green, and red dots (which are complex impedances) on the circles in Figure 3(d). Then, the red or the green dot can be matched to $r_s = 1$ with only one TL, as discussed previously, leading to the CVT in Figure 3(b). On the other hand, the blue dot on the constant-conductance circle can also be matched to $r_s = 1$ with only one TL, leading to the CCT in Figure 3(c). By convention, the impedance transformers in Figure 3(b) and (c) are called *CVTs* and *CCTs* [31], respectively.

In this case, the blue, green, and red dots on the half circles are the input impedances of z_{in_t} and z_{in_o} in Figure 3(a) and (b), which are

$$z_{in\_t} = z_t \frac{r_l + jz_t \tan\Theta_t}{z_t + jr_l \tan\Theta_t}, \tag{7a}$$

$$z_{in\_o} = \left(\frac{1}{r_l} + \frac{j\tan\Theta_o}{z_o}\right)^{-1}. \tag{7b}$$

The characteristic impedances of z_{ct} and z_{co} and the electrical lengths of Θ_{ct} and Θ_{co} in Figure 3(b) and (c) can be easily calculated by substituting (z_{in_t} and z_s) and (z_{in_o} and z_s) into (1) and (2) as

$$z_{ct} = CH(z_{in\_t},\ z_s),\ \Theta_{ct} = EL(z_{in\_t}, z_s), \tag{8a}$$

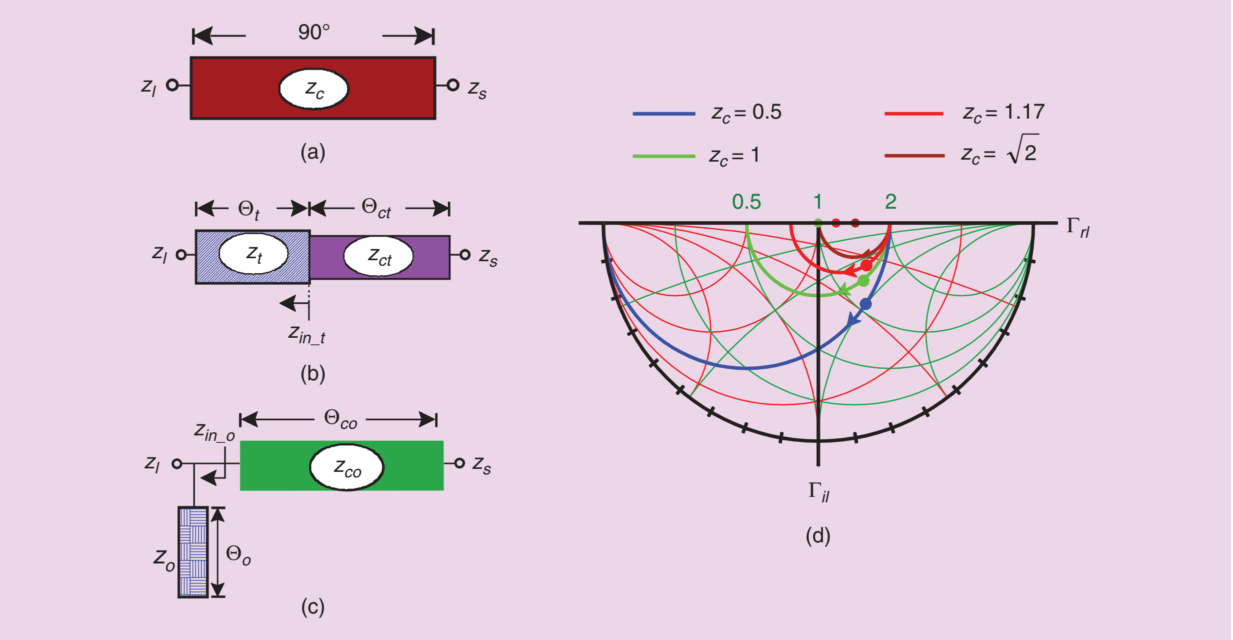

Figure 3. *The CVT and CCT. (a) A 90° impedance transformer. (b) A CVT. (c) A CCT. (d) The Smith chart for CVTs and CCTs.*

$$z_{co} = CH(z_{in\_o}, z_s), \Theta_{co} = EL(z_{in\_o}, z_s). \quad (8b)$$

For $r_l/r_s = 1.6$, the input impedances of z_{in_t} and z_{in_o} of the CVTs and CCTs in Figure 3(b) and (c) were calculated, fixing the characteristic impedances at $z_t = z_o = 1\,\Omega$ and varying Θ_t and Θ_o: they are expressed on the Smith chart in Figure 4. The input impedances of z_{in_t} of the CVTs are shown as blue dots on the blue circle (a constant-VSWR circle), while those of z_{in_o} of the CCTs are red dots on the red circle (a constant-conductance circle) in Figure 4, where the corresponding values of Θ_t and Θ_o are written. Both circles pass through $r = 1.6$ on the real axis of the Smith chart, as shown in Figure 4, where the three functions G_{f1}, G_{f2}, and G_{f3} (6) that define the allowed and forbidden regions are drawn. The hatched area is a forbidden region, while the spaces surrounded by the three functions are allowed regions. If a red or blue dot is in the forbidden region, the CVTs and CCTs can't be defined. Therefore, the values of Θ_t and Θ_o should not be too large; otherwise, they would enter the forbidden region. Additionally, phase angles are indicated with red, blue, and purple dotted circles crossing from left to right on the Smith chart.

In general, if the input impedance is located on a lower phase-angle circle, the bandwidth is wider [29]–[31]. For this reason, the bandwidth of the 20° CCT on the red circle is smaller than that of the 20° CVT. As mentioned, if a complex load of z_{in_t} and z_{in_o} is located on G_{f3}, the electrical lengths of Θ_{ct} or Θ_{co} are 90°, which is a quarter-wave impedance transformer, and Θ_{co} of the 15° CCT is smaller than Θ_{ct} of 15° CVT because the input impedance of the 15° CCT is located farther from G_{f3} than that of the 15° CVT. The exact values for the design parameters can be calculated using (8).

The design parameters of the CVTs and CCTs for $r_l/r_s = 1.6$ in Figure 4 are listed in Table 1, fixing $Z_T = z_t R_S = 50\,\Omega$ and $Z_O = z_o R_S = 50\,\Omega$ with $R_S = 50\,\Omega$ and varying the electrical lengths of Θ_t and Θ_o, where $Z_{CT} = z_{ct} R_S$ and $Z_{CO} = z_{co} R_S$. When $\Theta_t = \Theta_o = 30°$ in Table 1, the CVT is possible; however, the CCT is impossible because the input impedance of the CCT with $\Theta_o = 30°$ is already in the forbidden region, as shown in Figure 4. The six CVTs and CCTs in Table 1 were simulated at the design frequency of 3 GHz, and the frequency responses are plotted in Figure 5, where the bandwidths are proportional to the total electrical lengths of $\Theta_{ct} + \Theta_t$ or Θ_{co} and, in general, agree with the relation between the phase angles and the locations of the input impedances. Several CVTs and CCTs were fabricated and are depicted in Figure 6(a)–(d); the measured responses are compared in Figure 6(e), where the termination impedances of R_L are $1.6 * 50\,\Omega$, not $50\,\Omega$; therefore, impedance transformers are needed to measure them. The bandwidth of the 20° CVT is widest in Figure 6(e) because the total TL length is the longest, and its input impedance is located on the lowest phase-angle circle in Figure 4.

CVT3PDs and CCT3PDs

The impedance transformers CVT and CCT can be applied to 3-dB PDs, namely CVT3PDs and CCT3PDs.

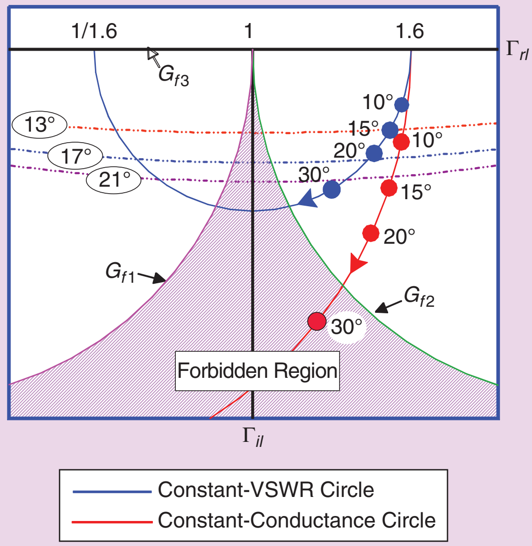

Figure 4. *The input impedances of z_{in_t} on a constant-VSWR circle and those of z_{in_o} on a constant-conductance circle.*

TABLE 1. The design parameters of CVTs and CCTs with $r_l/r_s = 1.6$.

CVTs	Z_{CT}	Θ_{ct}	CCTs	Z_{CO}	Θ_{co}
$\Theta_t = 10°$	64.3 Ω	69.4°	$\Theta_o = 10°$	67.9 Ω	57.4°
$\Theta_t = 15°$	65.7 Ω	59.1°	$\Theta_o = 15°$	75.9 Ω	42.7°
$\Theta_t = 20°$	68.2 Ω	48.7°	$\Theta_o = 20°$	95.9 Ω	28.2°
$\Theta_t = 30°$	82.4 Ω	27.1°	$\Theta_o = 30°$	X	X

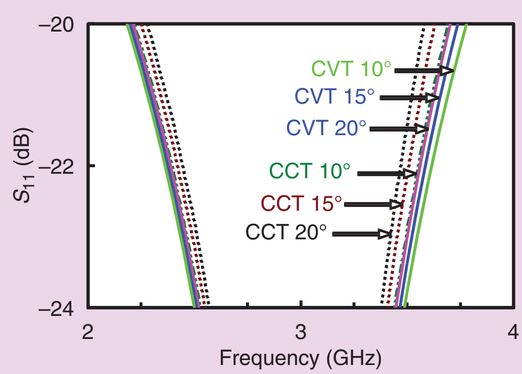

Figure 5. *The simulated frequency responses of CVTs and CCTs for $r_l/r_s = 1.6$.*

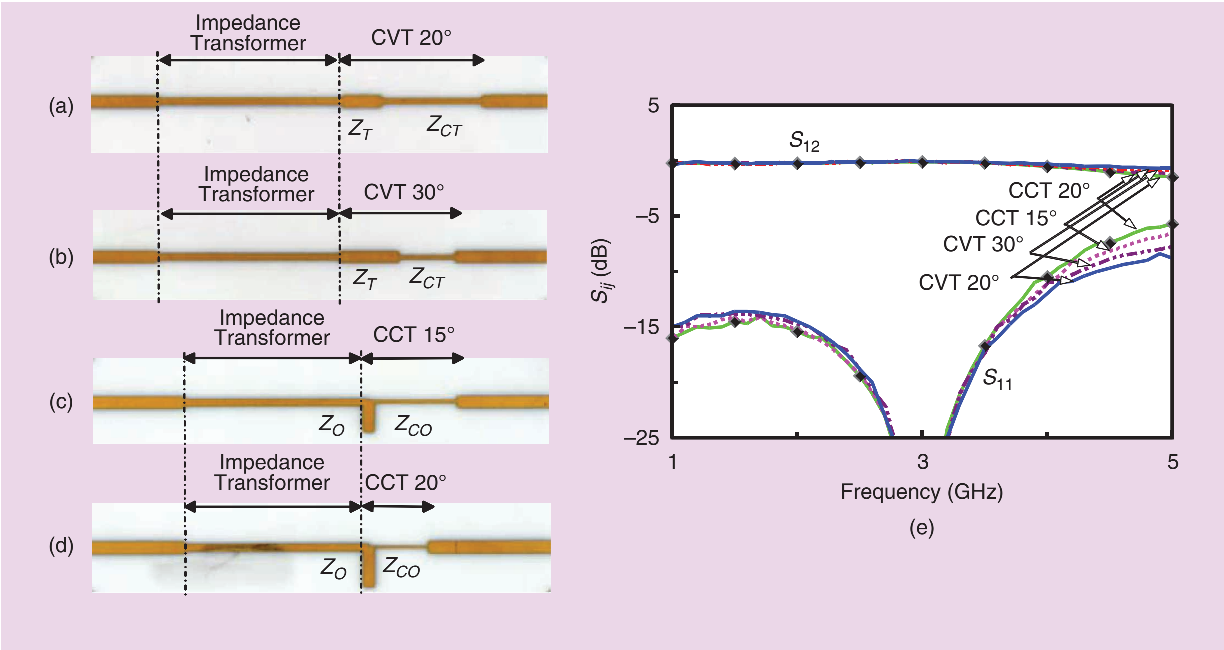

Figure 6. *The fabricated CVTs and CCTs and their frequency responses. (a) The fabricated 20° CVT. (b) The fabricated 30° CVT. (c) The fabricated 15° CCT. (d) The fabricated 20° CCT. (e) The compared measured frequency responses.*

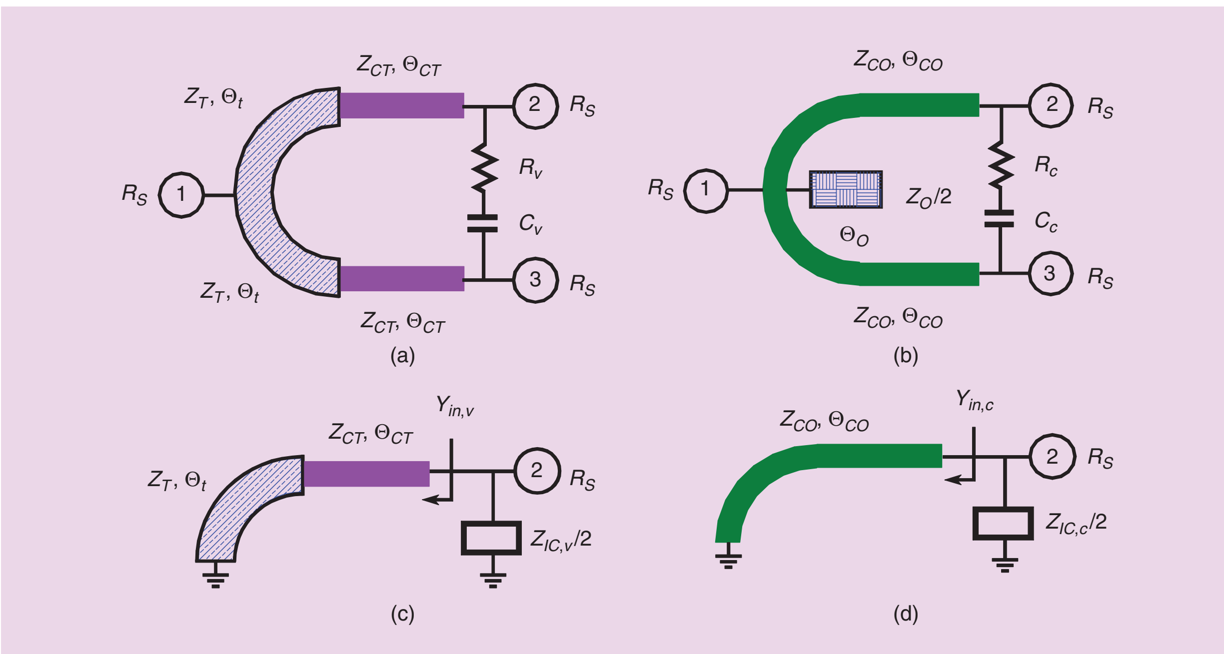

Figure 7. *(a) The CVT3PD. (b) The CCT3PD. (c) The odd-mode equivalent circuit of the CVT3PD. (d) The odd-mode equivalent circuit of the CCT3PD.*

For this purpose, $Z_L = R_L$ and $Z_S = R_S$ in Figure 3(b) and (c) should be 100 and 50 Ω, respectively; they are depicted in Figure 7(a) and (b). The even-mode equivalent circuits are those in Figure 3(b) and (c), and the odd-mode equivalent circuits are those in Figure 7(c) and (d), where the half of the isolation impedances $Z_{IC,v}/2$ and $Z_{IC,c}/2$ and the input admittances of $Y_{in,v}$ and $Y_{in,c}$ are indicated. The input admittances of $Y_{in,v}$ and $Y_{in,c}$ in Figure 7(c) and (d) are

$$Y_{in,v} = -jY_{CT}\frac{Y_T\cot\Theta_t - Y_{CT}\tan\Theta_{ct}}{Y_{CT} + Y_T\cot\Theta_t\tan\Theta_{ct}},\ Y_{in,c} = -jY_{CO}\cot\Theta_{co}, \quad (9)$$

where $Y_T = Z_T^{-1}$, $Y_{CT} = Z_{CT}^{-1}$, $Y_T = Z_T^{-1}$, $Y_O = Z_O^{-1}$, and $Y_{CO} = Z_{CO}^{-1}$.

For the isolation impedances $Z_{IC,v}/2$ and $Z_{IC,c}/2$, the following relations hold:

$$Y_{in,v} + \frac{2}{Z_{IC,v}} = \frac{1}{R_S}, \quad Y_{in,c} + \frac{2}{Z_{IC,c}} = \frac{1}{R_S}. \tag{10}$$

From (10), the isolation impedances of $Z_{IC,v}$ and $Z_{IC,c}$ are derived as

$$Z_{IC,v} = 2\left(\frac{1}{R_S} - Y_{in,v}\right)^{-1}, \quad Z_{IC,c} = 2\left(\frac{1}{R_S} - Y_{in,c}\right)^{-1}. \tag{11}$$

Based on the design formulas, one CVT3PD and one CCT3PD are designed at 1 GHz, and the architecture parameters are listed in Table 2. For the CVT3PD, if the characteristic impedance of Z_T and the electrical length of Θ_t in Figure 7(a) are arbitrarily selected as $Z_T = 30\,\Omega$ and $\Theta_t = 16°$, the values for Z_{CT} and Θ_{ct} can be calculated as $Z_{CT} = 136.3\,\Omega$ and $\Theta_{ct} = 21.5°$ using (8). Only $Z_T = 50\,\Omega$ is possible for [31] because the graphical method [31] uses the Smith chart normalized to $R_S = 50\,\Omega$. In this case, the isolation impedance of $Z_{IC,v}$ is calculated as $Z_{IC,v} = (61.9 - j48.6)\,\Omega$, which can be fabricated with a series connection of $R_v = 61.9\,\Omega$ and $C_v = 3.28$ pF at 1 GHz in Figure 7(a). In a similar way, one CCT3PD can be designed. For the CCT3PD, the open stub with $Z_O/2$ and Θ_o in Figure 7(b) can be replaced with a chip capacitor, and the value of C_s in Table 2 is the corresponding capacitance value at 1 GHz. Compared to conventional PDs with two 90° TLs, the total TL lengths are very small.

The CVT3PD and the CCT3PD in Table 2 were simulated at the design frequency of 1 GHz: the frequency responses are plotted in Figure 8, where the solid-line responses are those of the CVT3PD and the dotted lines are those of CCT3PD. Near-perfect frequency responses of the two PDs are achieved, and both frequency responses are similar to each other, even though the total TL length of the CCT3PD is less than that of the CVT3PD .

CVTs and CCTs in Forbidden Regions

CVTs and CCTs can be applied to complex impedance transformers where the termination impedances of z_l are located in forbidden regions. When the two complex impedances $z_l = (0.9 - j0.6)\,\Omega$ and $z_s = (1 - j0.3)\,\Omega$ are given, the complex impedance of z_l is located in a forbidden region, which can be known by substituting the two values into (3a). The two complex impedances and the three functions of G_{f_1}, G_{f_2}, and G_{f_3} (6) are drawn in Figure 9, with the complex impedance of z_s located where the three functions meet and z_l located outside the hatched regions. The hatched regions are indicated as allowed regions and may be divided into I^-, II^-, III^-, and IV^-, with the letter A of AI^-, AII^-, $AIII^-$, and AIV^- indicating allowed regions, the superscript minus sign meaning that x_s is negative, and the plus or minus sign located beside the notation indicating the sign of the electrical length of Θ. The positive or negative electrical length of Θ means $\Theta < 90°$ or $\Theta > 90°$, respectively, and, if z_l is located on the circle of G_{f_3}, $\Theta = 90°$. As mentioned previously, if the complex impedance of z_l is located outside the allowed regions, it is impossible to match z_l to z_s with only one TL. Therefore, the

TABLE 2. The design parameters for CVT3PDs and CCT3PDs with $R_S = 50\,\Omega$.

CVT3PDs terminated in $R_S = 50\,\Omega$ at 1 GHz
$Z_T = 30\,\Omega$, $\Theta_t = 16°$, $Z_{CT} = 136.3\,\Omega$, $\Theta_{ct} = 21.5°$
$Z_{IC,v} = (61.9 - j48.6)\,\Omega \rightarrow R_v = 61.9\,\Omega$, $C_v = 3.3$ pF
CCT3PDs terminated in $R_S = 50\,\Omega$ at 1 GHz
$Z_o = 40\,\Omega$, $\Theta_o = 19°$, $Z_{CO} = 138.9\,\Omega$, $\Theta_{CO} = 22.7°$, $C_s = 2.7$ pF
$Z_{IC,c} = (57.4 - j\,49.4)\,\Omega \rightarrow R_c = 57.4\,\Omega$, $C_c = 3.2$ pF

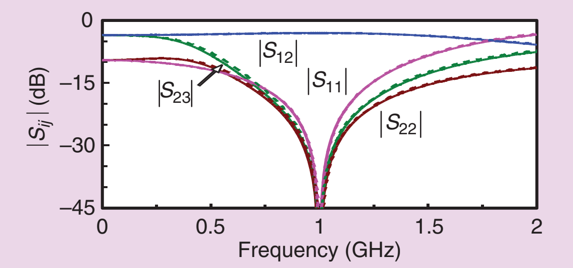

Figure 8. *The frequency responses of the CVT3PD (solid lines) and CCT3PD (dotted lines).*

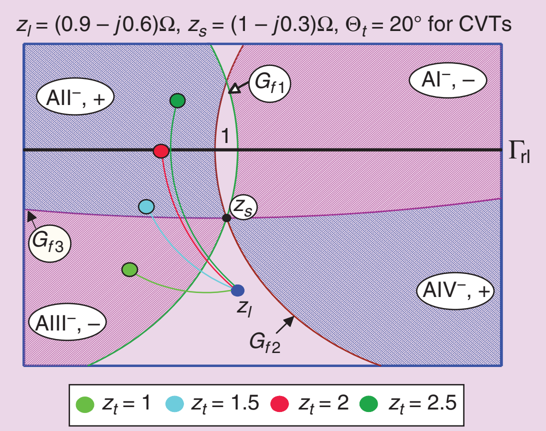

Figure 9. *An example of z_l located in a forbidden region for CVTs.*

Conventional methods can't treat all possible complex termination impedances, due to lack of an available systematic design method.

load of z_l should be moved along a TL or an open stub. In this case, moving only one TL for CVTs is detailed further.

When Θ_t is fixed at 20° and z_t is allowed to vary, as shown in Figure 9, the resulting input impedances of z_{in_t} are described as four different dots. When $z_t = 1$, the input impedance of z_{in_t} is still in the region of $\mathrm{AIII}^-, -$; therefore, the electrical length of Θ_{ct} in Figure 3(b) is negative or greater than 90°. When $z_t = 1.5$, the input impedance of z_{in_t} is in the region of $\mathrm{AII}^-, +$. The electrical length of Θ_{ct} is positive but close to 90° because the point of z_{in_t} with $z_t = 1.5$ is located close to the function of G_{f3}. When $z_t = 2$, the input impedance of z_{in_t} is located farther from the function of G_{f3}. Therefore, the electrical length of Θ_{ct} should be less than that with $z_t = 1.5$. In this way, the three functions give all the information for z_{ct} and Θ_{ct}; the exact values for z_{ct} and Θ_{ct} for the CVTs can be calculated using (8a), as well.

Small-Phase-Delay PDs [32], [33]

When $\Theta_o = 25°$ of the CCT in Figure 3(c) for $r_l/r_s = 2$, the characteristic impedance of $Z_{CO} = z_{co}R_S$ with $R_S = 50\,\Omega$ is already $195\,\Omega$, an infeasible characteristic impedance for a microstrip format. When $r_l/r_s = 2$, the input impedance of z_{in_o} of the CCT in Figure 3(c) is expressed for $\Theta_o = 25°$ as a blue dot in Figure 10(a), and one TL can match the blue dot and the origin, $r_s = 1$. In this case, referring to [5, Figs. 3(b) and 4(b)], [31], the perpendicular bisector of the line connecting the two complex impedances [or the blue dot and the origin in Figure 10(a)] intersects the real axis, and the point indicates the characteristic impedance of z_{co} in Figure 3(c), or 3.9, implying $3.9 * 50 = 195\,\Omega$.

To alleviate the infeasible characteristic impedance problem, a short stub needs to be connected to z_s, as shown in Figure 10(b), where the characteristic impedance and electrical length of the short stub are assumed to be z_{sh} and Θ_{sh}, respectively. Two input impedances of z_{in_o} and z_{in_sh} are indicated in Figure 10(b). The impedance transformer in Figure 10(b) is suggested in [32], but the design formulas are derived based on full-port scattering parameters, requiring complicated derivation process. Using (1) and (2), the design formulas can be derived very easily. The input impedance of z_{in_sh} is

$$z_{in\_sh} = \left(\frac{1}{r_s} + \frac{1}{jz_{sh}\tan\Theta_{sh}}\right)^{-1}. \tag{12}$$

So the characteristic impedance of z_{cos} and the electrical length of Θ_{cos} are

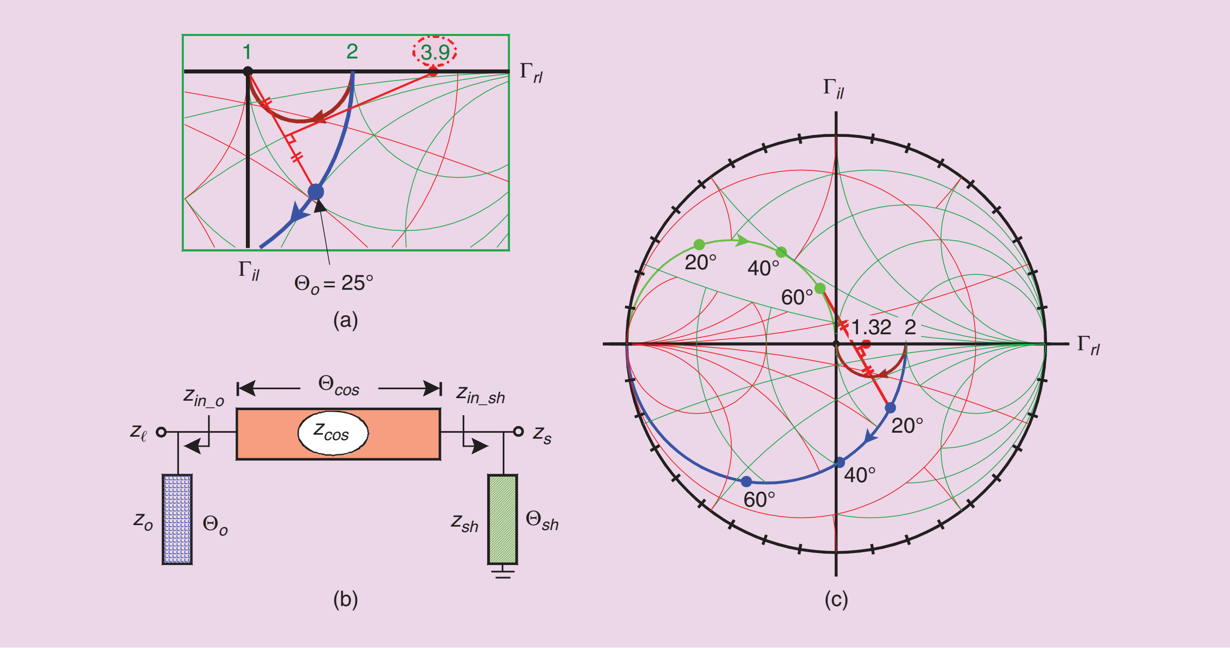

Figure 10. *The complex impedance transformer for small phase delays [32]. (a) For $r_l/r_s = 2$, the approximate characteristic impedance of z_{co} equals that of the CCT with $\Theta_o = 25°$ in Figure 3(c). (b) The complex impedance transformer for small phase delays. (c) The Smith chart for the small phase delay complex impedance transformers in (b).*

$$z_{\cos} = CH(z_{in\_o}, z_{in\_sh}), \quad \Theta_{\cos} = EL(z_{in\_o}, z_{in\_sh}), \qquad (13)$$

where z_{in_o} is in (7b).

The blue circle in Figure 10(c) is a constant-conductance circle passing through $r = 2$ or $g = 0.5$, while the green circle is also a constant-conductance circle passing through $r = 1$ or $g = 1$. With $z_{sh} = z_o = 1$ in Figure 10(b), the input impedances of z_{in_o} and z_{in_sh} are expressed, varying Θ_o and Θ_{sh} as the blue and green dots on the blue and green constant-conductance circles, respectively. When $\Theta_o = 20°$ and $\Theta_{sh} = 60°$, to match z_{in_o} to z_{in_sh}, one TL is sufficient, and the characteristic impedance of $z_{\cos}$ is only 1.32 [see Figure 10(c)], which is far less than the 3.9 in Figure 10(a).

The PD is depicted in Figure 11(a), where the open stubs and short stubs are expressed as the two admittance values Y_c and Y_d, respectively, and the isolation circuit with isolation admittance of Y_b is connected between ports ② and ③. If $\Theta_o = 32.7°$ and $\Theta_{sh} = 53.9°$ are determined with $Z_O = z_o R_S = 50\,\Omega$ and $Z_{SH} = z_{sh} R_S = 50\,\Omega$, the other design parameters can be easily calculated as $Z_{COS} = z_{\cos} R_S = 110\,\Omega$ and $\Theta_{\cos} = 12.7°$ using (13); the isolation admittance of Y_b can be calculated similarly to (11) as $(0.01 + j0.027)\,℧$. The fabricated PD [32] is displayed in Figure 11(b), where the design frequency is 0.7 GHz, and the admittance values Y_c and Y_d are fabricated with the chip capacitor and inductors, respectively. The frequency responses are plotted in Figure 11(c). The size is relatively small compared to CVTs and CCTs, and the phase delay is only 20°, leading to a relatively narrow bandwidth in Figure 11(c). To enlarge the bandwidths and fabricate compact sizes, another type of complex impedance transformer is necessary, as discussed in the next section.

Ultracompact and Wideband VHF and UHF PDs [34]

Another application of complex impedance transformers concerns ultracompact and wideband very-high-frequency (VHF) and ultrahigh-frequency (UHF) 3-dB PDs. A PD with the equal termination impedances of R_S in Figure 12(a) consists of two pairs of TLs, one open stub with the characteristic impedance $Z_o/2$ and the electrical length of Θ_o and two identical inductances of L. The characteristic impedance and the electrical length of the TL located close to port ① are Z_T and Θ_T, respectively, while those of the TL close to port ② are Z_{Ta} and Θ_{Ta}. The even-mode equivalent circuit is depicted in Figure 12(b), where two input impedances of Z_L and Z_S are indicated, and the isolation impedance is realized using a series connection with a resistor of R_{ic} and a capacitor of C_{ic}, as in Figure 12(a). The two input impedances of Z_L and Z_S in Figure 12(b) are

The fabricated PD may be regarded as the smallest ever recorded using low-cost microstrip technology versus wide bandwidth (58%).

$$Z_L = \left(j\frac{1}{Z_o}\tan\Theta_o + \frac{1}{2R_S}\right)^{-1},$$
$$Z_S = j\omega L + Z_{Ta}\frac{R_S + jZ_{Ta}\tan\Theta_{Ta}}{Z_{Ta} + jR_S\tan\Theta_{Ta}}. \qquad (14)$$

The characteristic impedance Z_T and electrical length Θ_T can be easily derived as $Z_T = CH(Z_L, Z_S)$ and $\Theta_T = EL(Z_L, Z_S)$ in (1) and (2); the isolation impedance of Z_{ic} in Figure 12(c) can be calculated similarly to (11). The isolation impedances were calculated, varying ωL and Θ_o and fixing $R_S = Z_o = 50\,\Omega$, $Z_{Ta} = 105\,\Omega$, and $\Theta_{Ta} = 4°$. The calculation results are plotted in Figure 12(c) and (d), the resistances of R_{ic} are in Figure 12(c), while the capacitance values of C_{ic} at 0.1 GHz are in Figure 12(d). Both values decrease with Θ_o.

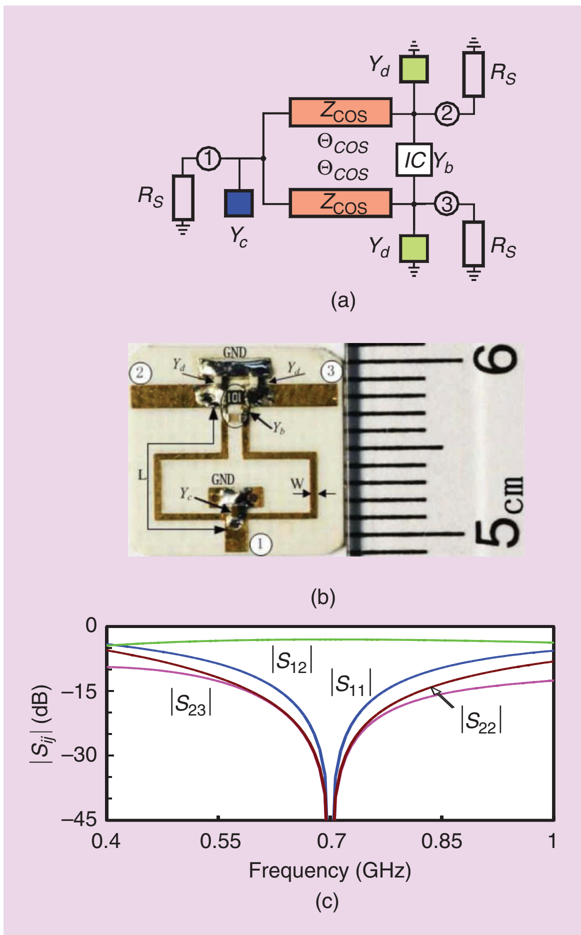

Figure 11. *(a) The PD configuration. (b) The fabricated PD [32]. (c) The simulated frequency responses. GND: ground.*

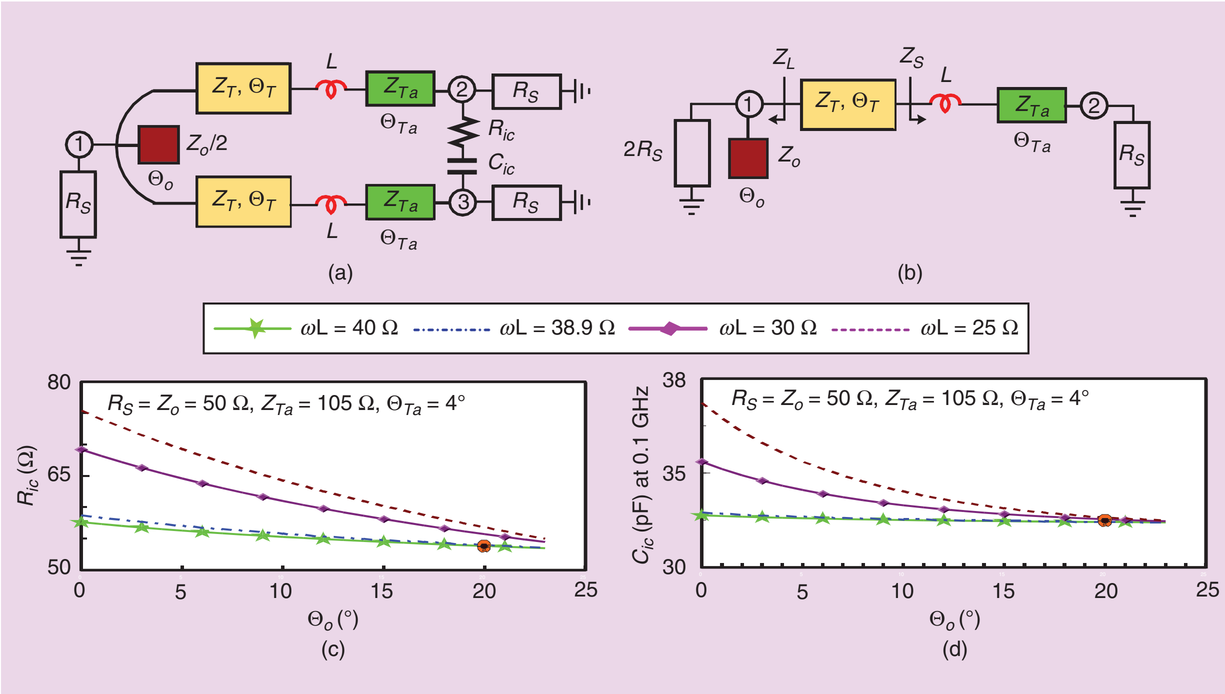

Figure 12. *The ultracompact and wideband PD. (a) The PD topology. (b) The even-mode equivalent circuit. (c) The isolation resistances. (d) The isolation capacitances at 0.1 GHz.*

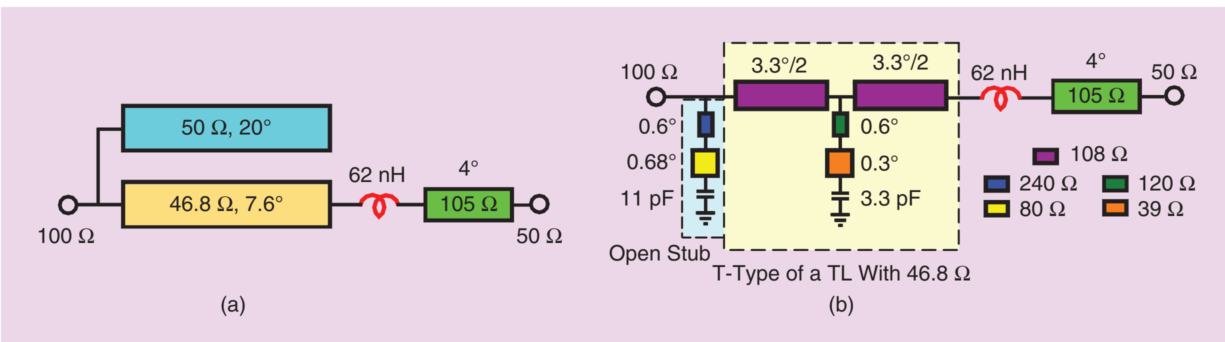

Figure 13. *The designed even-mode equivalent circuit. (a) The design parameters of the even-mode equivalent circuit. (b) The compact even-mode equivalent circuit.*

Design and Measurements

The PD in Figure 12(a) was designed at 100 MHz and fabricated on a substrate (RT/duroid 5880, $\varepsilon_r = 2.2$, $H = 62$ mil). The conventional PD consists of two 90° TLs with a characteristic impedance of 70.7 Ω. At 100 MHz and 1 GHz, the physical lengths of the 90° TL on the substrate are 555.4 and 55.5 mm, respectively, requiring a not-so-small occupied area, even at 1 GHz. Thus, the design of the PD at 100 MHz focuses on achieving a compact size, and a sophisticated design method is required. For this, the final values for Z_T and Θ_T should be as low as possible to further reduce the TLs with Z_T and Θ_T, keeping the inherent bandwidths. After considering all the possible relations for compact size, $Z_{Ta} = 105\ \Omega$ and $\Theta_{Ta} = 4°$ along with $Z_O = 50\ \Omega$ were arbitrarily selected, referring to [34, Figs. 2–4]. With available chip resistors, capacitors, and inductors, the suitable solutions for ωL and Θ_o can be found by sweeping the isolation impedance values in Figure 12(c) and (d) as $\omega L = 38.9\ \Omega$ ($L = 62$ nH) and $\Theta_o = 20°$ [see the red dots in Figure 12(c) and (d)]. Then, the final values for Z_T and Θ_T can be calculated as $Z_T = 46.8\ \Omega$ and $\Theta_T = 7.6°$ using the two functions of $CH(Z_L, Z_S)$ and $EL(Z_L, Z_S)$ in (1) and (2), respectively.

The design parameters for the even-mode circuit are shown in Figure 13(a). The open stub with $Z_o = 50\ \Omega$ and $\Theta_o = 20°$ can be replaced by a chip capacitor with

11.58 pF at $f_0 = 100$ MHz. However, there is no such chip capacitor value, and soldering is also a problem. The open stub can be reduced to a stepped-impedance open stub with thin and wide TLs and an available chip capacitor of 11 pF, as shown in Figure 13(b), where the characteristic impedances of the thin and wide TLs are 240 and 80 Ω, respectively. Since two identical stepped-impedance open stubs are connected in parallel for the final PD in Figure 12(a), the characteristic impedances of 240 and 80 Ω become half values, and the capacitance of 11 pF is doubled.

Since the characteristic impedance of Z_T is still 46.8 Ω in Figure 13(a), the TL with Z_T and Θ_T can be further reduced to a T-type consisting of two identical TLs with a characteristic impedance of 108 Ω, electrical length of 3.3°/2, and one open stub. Similarly, the open stub of the T-type is also reduced and realized as the stepped-impedance open stub with an available chip capacitor of 3.3 pF, as shown in Figure 13(b) [35]. The TL with Z_T is 7.6° long in Figure 13(a), while the total TLs of the T-type are only 3.3° long in Figure 13(b). Nevertheless, the bandwidth of the T-type does not shrink, referring to [36, Fig. 10].

The fabricated PD is shown in Figure 14(a), and the measured responses are in Figure 14(b), where the isolation impedance is realized with an available chip resistor at 54.2 Ω and a capacitor at 32 pF. The measured 15-dB return-loss bandwidth of $|S_{11}|$ is 58% (120 − 72 MHz = 58 MHz). The measured power division of $|S_{21}|$ is −3.22 dB, and $|S_{31}| = -3.33$ dB, while $|S_{11}| = -34.7$ dB, and the isolation of $|S_{23}| = -22.6$ dB is achieved at 100 MHz. The total TLs of the fabricated PD are only 14.6° long, and the measured bandwidth is roughly 58%, leading to a 99.3% size reduction compared to conventional approaches with two 90° TLs. In terms of size/bandwidth, the fabricated PD in Figure 14(a) may be regarded as the smallest ever recorded using low-cost microstrip technology versus wide bandwidth (58%).

Since complex impedance transformers are basic elements, diverse applications may be expected for wireless power transfer systems.

Conclusions

In this article, a simple and powerful design method was suggested for complex impedance transformers. The study focused on the simplest circuit with only one TL, and the design was tested for both complex termination impedances. However, there are design restrictions, such as imaginary values of characteristic impedances and all possible complex termination impedances. To solve such problems, allowed and forbidden regions were defined in the impedance domain, and three mapping functions were derived for the reflection-domain analyses. As examples of applications for complex impedance transformers with only one TL, we introduced easy and better design methods for CVTs and CCTs [31] and small phase delay PDs [32], [33]. As a further application, an ultracompact and wideband 3-dB PD was designed and fabricated. The total TLs of the PD [34] are only 14.6° long, and the measured bandwidth is approximately 58%, leading to a 99.3% size reduction compared to conventional PDs with two 90° TLs. In terms of size versus bandwidth, the fabricated PD is the smallest ever recorded (based on low-cost microstrip technology). Since complex impedance transformers are basic elements, diverse applications may be expected for wireless power transfer systems, PDs (including the

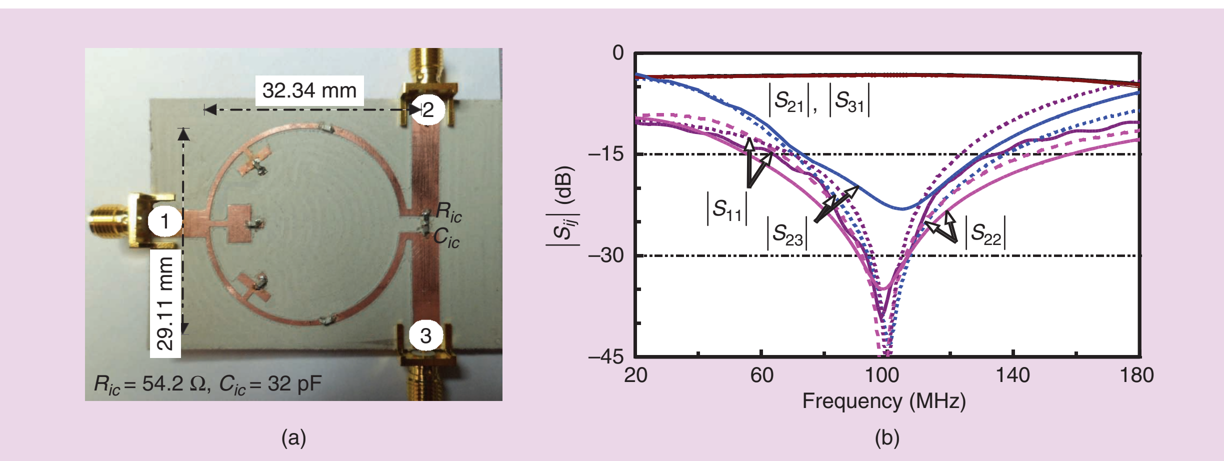

Figure 14. *The fabricated compact PD and its frequency responses. (a) The fabricated compact PD. (b) The measured (solid lines) and predicted (dotted lines) frequency responses.*

three examples treated in this article), and ring hybrids with harmonic suppressions and filters.

References

[1] H.-R. Ahn, I.-S. Chang, and S.-W. Yun, "Miniaturized 3-dB ring hybrid terminated by arbitrary impedances," *IEEE Trans. Microw. Theory Techn.*, vol. 42, no. 12, pp. 2216–2221, Dec. 1994. doi: 10.1109/22.339745.

[2] H.-R. Ahn, I. Wolff, and I.-S. Chang, "Arbitrary termination impedances, arbitrary power division and small-sized ring hybrids," *IEEE Trans. Microw. Theory Techn.*, vol. 45, no. 12, pp. 2241–2247, Dec. 1997. doi: 10.1109/22.643824.

[3] H.-R. Ahn and M. M. Tentzeris, "Comments on 'A theorem on asymmetric structure based on rat-race coupler'," *IEEE Microw. Compon. Lett.*, vol. 29, no. 10, pp. 696–698, 2019. doi: 10.1109/LMWC.2019.2919515.

[4] J. Bito, S. Jeong, and M. M. Tentzeris, "A novel heuristic passive and active matching circuit design method for wireless power transfer to moving objects," *IEEE Trans. Microw. Theory Techn.*, vol. 65, no. 4, pp. 1094–1102, Apr. 2017. doi: 10.1109/TMTT.2017.2672544.

[5] H.-R. Ahn, "Complex impedance transformers consisting of only TLs," *IEEE Trans. Microw. Theory Techn.*, vol. 60, no. 7, pp. 2073–2084, July 2012. doi: 10.1109/TMTT.2012.2197022.

[6] H.-R. Ahn and S. Nam, "3-dB power dividers with equal complex termination impedances and design methods for controlling isolation circuits," *IEEE Trans. Microw. Theory Techn.*, vol. 61, no. 11, pp. 3872–3883, Nov. 2013. doi: 10.1109/TMTT.2013.2281101.

[7] H. Jasik, *Antenna Engineering Handbook*, 1st ed. New York: McGraw-Hill, 1961, ch. 31.

[8] T. A. Milligan, "Transmission-line transformation between arbitrary impedances," *IEEE Trans. Microw. Theory Techn.*, vol. 24, no. 3, p. 159, Mar. 1976. doi: 10.1109/TMTT.1976.1128802.

[9] M. H. N. Potok, "Comments on 'Transmission-line transformation between arbitrary impedances'," *IEEE Trans. Microw. Theory Techn.*, vol. 25, no. 1, p. 77, Jan. 1977. doi: 10.1109/TMTT.1977.1129040.

[10] Q. He, Y. Liu, M. Su, and Y. Wu, "A compact dual-frequency transformer for frequency-dependent complex impedance load," in *Proc. Asia Pacific Microwave Conf.*, Dec. 2012, pp. 1241–1243. doi: 10.1109/APMC.2012.6421882.

[11] Y. Liu, Y. Zhao, S. Liu, Y. Zhou, and Y. Chen, "Multi-frequency impedance transformers for frequency-dependent complex loads," *IEEE Trans. Microw. Theory Techn.*, vol. 61, no. 9, pp. 3225–3235, Sept. 2013. doi: 10.1109/TMTT.2013.2274779.

[12] O. Manoochehri, A. Asoodeh, and K. Forooraghi, " Π-model dual-band impedance transformer for unequal complex impedance loads," *IEEE Microw. Compon. Lett.*, vol. 25, no. 4, pp. 238–240, Apr. 2015. doi: 10.1109/LMWC.2015.2400933.

[13] M. A. Nikravan and Z. Atlasbaf, "T-section dual-band impedance transformer for frequency-dependent complex impedance loads," *Electron. Lett.*, vol. 47, no. 9, pp. 551–553, Apr. 2011. doi: 10.1049/el.2010.7452.

[14] M. A. Maktoomi, R. Gupta, and M. S. Hashmi, "A dual-band impedance transformer for frequency-dependent complex load incorporating an L-type network," in *Proc. Asia-Pacific Microwave Conf.*, Dec. 2015, vol. 1, pp. 1–3. doi: 10.1109/APMC.2015.7411641.

[15] F. Giannini and L. Scucchia, "A complete class of harmonic matching networks: Synthesis and application," *IEEE Trans. Microw. Theory Techn.*, vol. 57, no. 3, pp. 612–619, Mar. 2009. doi: 10.1109/TMTT.2009.2013319.

[16] X. F. Dylan, T. Bespalko, and S. Boumaiza, "Novel dual-band matching network topology and its application for the design of dual-band class J power amplifiers," in *Proc. IEEE MTT-S Int. Microwave Symp. Dig.*, Montreal, QC, June 2012. pp. 1–3. doi: 10.1109/MWSYM.2012.6259644.

[17] M.-L. Chuang and M.-T. Wu, "General dual-band impedance transformer with a selectable transmission zero," *IEEE Trans. Compon., Package., Manuf. Technol.*, vol. 6, no. 7, pp. 1113–1119, July 2016. doi: 10.1109/TCPMT.2016.2572220.

[18] P. Colantonio, F. Giannini, and L. Scucchia, "A new approach to design matching networks with distributed elements," in *Proc. 15th Int. Conf. Microwave Radar and Wireless Communications*, May 2004, vol. 3, pp. 811–814. doi: 10.1109/MIKON.2004.1358480.

[19] L.-C. Tsai, "Triple-band impedance transformers using equal-length serial transmission lines," *IET Microw., Antennas. Propag.*, vol. 10, no. 5, pp. 568–573, 2016. doi: 10.1049/iet-map.2015.0633.

[20] M.-G. Chen, C.-W. Tang, T.-B. Hou, and J.-W. Wu, "Adopting the broadside coupled line for the design of an impedance transformer," in *Proc. IEEE MTT-S Int. Microwave Symp.*, 2011, pp. 1–4. doi: 10.1109/MWSYM.2011.5972707.

[21] M.-G. Chen, T.-B. Hou, and C.-W. Tang, "Design of planar complex impedance transformers with the modified coupled line," *IEEE Trans. Compon. Packag. Manuf. Technol.*, vol. 2, no. 10, pp. 1704–1710, Oct. 2012. doi: 10.1109/TCPMT.2012.2207457.

[22] T. Jensen, V. Zhurbenko, V. Krozer, and P. Meincke, "Coupled transmission Lines as impedance transformer," *IEEE Trans. Microw. Theory Techn.*, vol. 55, no. 12, pp. 2957–2965, Dec. 2007. doi: 10.1109/TMTT.2007.909617.

[23] H.-R. Ahn and M. M. Tentzeris, "Wideband and compact impedance-transforming 90° DC blocks with symmetric coupled transmission-line sections," *IEEE Trans. Compon. Packag. Manuf. Technol.*, vol. 9, no. 1, pp. 80–87, Jan. 2019. doi: 10.1109/TCPMT.2018.2838327.

[24] H.-R. Ahn and T. Itoh, "Impedance-transforming symmetric and asymmetric DC blocks," *IEEE Trans. Microw. Theory Techn.*, vol. 58, no. 9, pp. 2463–2474, Sept. 2010. doi: 10.1109/TMTT.2010.2058936.

[25] L. T. Hall, H. J. Hansen, B. R. Davis, and D. Abbott, "Performance analysis of a series transformer for complex impedance matching," *Microw. Opt. Technol. Lett.*, vol. 45, no. 6, pp. 491–494, June 2005. doi: 10.1002/mop.20861.

[26] I. J. Bahl, "Broadband and compact impedance transformers for microwave circuits," *IEEE Microw. Mag.*, vol. 7, no. 4, pp. 56–62, Aug. 2006. doi: 10.1109/MMW.2006.1663990.

[27] S. J. Orfanidis, "Electromagnetic waves and antennas," Department of Electrical and Computer Engineering, Rutgers University, Piscataway, NJ, 2016. [Online]. Available: http://eceweb1.rutgers.edu/~orfanidi/ewa/ewa-1up.pdf

[28] H.-R. Ahn and M. M. Tentzeris, "Complex impedance transformers based on allowed and forbidden regions," *IEEE Access*, vol. 7, pp. 39,288–39,298, Mar. 2019. doi: 10.1109/ACCESS.2019.2906189.

[29] H.-R. Ahn, *Asymmetric Passive Components in Microwave Integrated Circuits*. Hoboken, NJ: Wiley, 2006.

[30] H.-R. Ahn, "Modified asymmetric impedance transformers (MCCTs and MCVTs) and their application to impedance-transforming three-port 3-dB power dividers," *IEEE Trans. Microw. Theory Techn.*, vol. 59, no. 12, pp. 3312–3321, Dec. 2011. doi: 10.1109/TMTT.2011.2171708.

[31] H.-R. Ahn and I. Wolff, "General design equations, small-sized impedance transformers, and their applications to small-sized three-port 3-dB power dividers," *IEEE Trans. Microw. Theory Techn.*, vol. 49, no. 7, pp. 1277–1288, July 2001. doi: 10.1109/22.932248.

[32] C. Miao, J. Yang, G. Tian, X. Zhang, and W. Wu, "Novel sub-miniaturized Wilkinson power divider based on small phase delay," *IEEE Microw. Compon. Lett.*, vol. 24, no. 10, pp. 662–664, Oct. 2014. doi: 10.1109/LMWC.2014.2340580.

[33] H.-R. Ahn and M. M. Tentzeris, "Comments on 'Novel sub-miniaturized Wilkinson power divider based on small phase delay'," *IEEE Microw. Compon. Lett.*, vol. 29, no. 6, p. 439, June 2019. doi: 10.1109/LMWC.2019.2902955.

[34] H.-R. Ahn and M. M. Tentzeris, "Ultra-compact and wideband V(U)HF 3-dB power dividers consisting of novel asymmetric impedance transformers," *IEEE Access*, vol. 7, pp. 76,367–76,375, June 2019. doi: 10.1109/ACCESS.2019.2921332.

[35] H.-R. Ahn and S. Nam, "New design formulas for impedance-transforming 3-dB Marchand baluns," *IEEE Trans. Microw. Theory Techn.*, vol. 59, no. 11, pp. 2816–2823, Mar. 2013. doi: 10.1109/TMTT.2011.2164618.

[36] H.-R. Ahn and S. Nam, "Compact microstrip 3-dB coupled-line ring and branch-line hybrids with new symmetric equivalent circuits," *IEEE Trans. Microw. Theory Techn.*, vol. 61, no. 3, pp. 1067–1078, Mar. 2013. doi: 10.1109/TMTT.2013.2241783.